

Crédit photo : H. Bonnard / P'

Étude expérimentale des chargements hydrodynamiques générés par les impacts de vagues déferlantes sur des éoliennes flottantes SPAR

Experimental investigation of the hydrodynamic loads induced by breaking wave impacts on a SPAR-type floating offshore wind turbine

F. Hulin^(1,2,3), A. Tassin⁽²⁾, J.F. Filipot⁽¹⁾, N. Jacques⁽³⁾

⁽¹⁾France Énergies Marines, Plouzané, France

⁽²⁾Ifremer, RDT, F-29280 Plouzané, France

⁽³⁾ENSTA Bretagne, UMR CNRS 6027, IRDL, 29806 Brest Cedex 09, France

Résumé

Des impacts de vagues déferlantes sur un cylindre segmenté mobile représentant une éolienne flottante ont été réalisés durant le projet DIMPACT. Ils visent à mieux caractériser les efforts d'impact générés et à les relier aux caractéristiques de la vague incidente ainsi qu'à l'attitude et aux mouvements de la maquette. Les paramètres étudiés sont la distance entre le point de déferlement et la face avant du cylindre, l'assiette de la maquette et sa vitesse horizontale. Une attention particulière a été donnée à la caractérisation des vagues incidentes.

Summary

Within the DIMPACT project, which aims at better characterizing impact forces generated by breaking waves on floating offshore wind turbines (FOWT), breaking wave impacts were carried out at Ifremer's wave flume on a mobile segmented SPAR-type FOWT model to study the influence of the mockup attitude and motion on the impact forces. The investigated parameters are the distance between the breaking location and the front face of the cylinder, the pitch angle of the cylinder and the horizontal speed of the cylinder. An important part of the work consisted in accurately characterizing the shape of the impacting waves.

I – Introduction

Breaking wave impacts are responsible for much higher loads on offshore wind turbines than steep non-breaking waves [3]. It is thus of importance to consider them during the design of floating offshore wind turbines (FOWT). Many experiments have been carried out to determine the impact forces generated by breaking waves. These experiments can be subdivided into two groups. First, a statistical approach considers a structure which is placed in a steep irregular wave field. The breaking occurrences are counted and the associated impact force is registered. This approach allows to obtain statistics concerning the breaking wave forces. Secondly, a deterministic approach consists in experiments in which the wave breaking position is known in advance. The structure is then placed close to the breaking position to generate impacts and to measure the exerted forces.

The first approach [8, 6, 12] allows to link a given sea state to a non-exceedance breaking force. Paulsen et al. [8] proposed a formula based on long time wave basin experiments to compute the maximum expected wave impact force on a wind turbine for a given sea state. Their experiments were conducted with different wave spectra, with and without currents and with different types of seabeds. In the second approach, particular breaking waves are linked to their impact forces. The wave characteristics (e.g. free surface profile, crest speed and elevation) are often better known. The influence of the impact parameters, such as the wave shape or the mockup attitude, can be studied. Wienke and Oumeraci [14] measured the impact force generated by phase-focused waves on a cylinder with a diameter of 0.7 m. Impacts were carried out with the cylinder inclined in both directions to study the influence on the wave impact force. A wide range of angles, going from -45° to $+45^\circ$ was covered. Other authors [15, 7, 11] studied the influence of the location of breaking with respect to the cylinder position. Zhou et al. [15] showed that impacts can occur only if the distance between the cylinder and the breaking location is in a certain interval. The impact characteristics greatly depend on the cylinder location. Only pressure data were recorded during the experiments of [15] and [7]. The evolution of the maximum impact force as a function of the distance between the cylinder and the breaking location is presented in [11] for a plunging wave, a mild plunging wave and a spilling wave. Breaking wave impacts on a moving cylinder were carried out by Saincher et al. [10]. The aim was to study the effect of currents on wave loadings. Only mockup motions in the direction opposite to the wave propagation were considered.

Different experimental setups have been used to characterize breaking wave impact loads. The most common approach consists in measuring the total force on the structure. It may be done by fixing the cylinder to the bottom of the tank or to a structure hanging over the flume using force transducers. Measurements are done at the top, at the bottom or at both ends of the structure [8, 14, 5, 2]. While this type of approach only allows a global measurement of the hydrodynamic force, more local approaches have been used to measure the spatial distribution of the hydrodynamic loads. For instance, several square force panels were used in [6] while circular sections were used in [13]. Half rings were used in [11]. Some experimental campaigns [15, 7] relied solely on pressure measurements.

The development of FOWTs, which are set in movement by waves, currents and wind loads, requires to more precisely determine the influence of the mockup attitude and motion on breaking wave impact loads. Within the DIMPACT project, wave impacts on a mobile segmented cylinder were carried out to measure the wave impact loads along the structure. The mockup was fixed to a six degrees-of-freedom motion generator. This allowed to easily modify the mockup attitude from one test to the other, as well as to carry out impact tests with a moving mockup. Different wave cases were generated to



FIGURE 1 – Overview of the mockup mounted over the flume

account for the variety of breaking waves that may be encountered at a given site. An important piece of work was devoted to the experimental characterization of the impacting breaking waves. The free surface profile evolution was measured using a high-speed video camera. The paper is organized as follows. The experimental setup is described in section II. Section III presents the breaking wave generation methodology and a comparison between measurements and the numerical simulations carried out with a numerical wave tank [4]. Section IV presents the loads measured on the mockup. Section V presents the influence of different impact parameters on the impact loads.

II – Experimental setup

II – 1 Wave flume

The experiments were carried out at Ifremer’s wave flume. It is equipped with a segmented piston-type wave generator. An absorbing beach is present at the other end. The flume is 40.5 m long from generator to beach, 2 m deep at the wave generator and 4 m wide. The flume bottom presents a slope of -0.5 % in the longitudinal and transversal directions (water depth increases toward the beach). It is filled with sea water. An overview of the experimental setup is depicted in figure 1.

II – 2 Presentation of the mockup

The instrumented mockup consists in a segmented cylinder which is 1.8 m high and whose diameter is equal to 40 cm. The mockup is fixed to a hanging frame through an hexapod, as depicted in figure 1. The use of the hexapod allows to precisely control the mockup position and motion. The mockup is made out of six different segments, as depicted in figure 2. A technical drawing of the mockup is shown in figure 3. Sections S_1 to S_3 are instrumented with MCS10-025 type and section S_4 with MCS10-010 type HBM load cells. The force transducers on sections S_1 to S_3 have a 5 kN nominal range and a 2

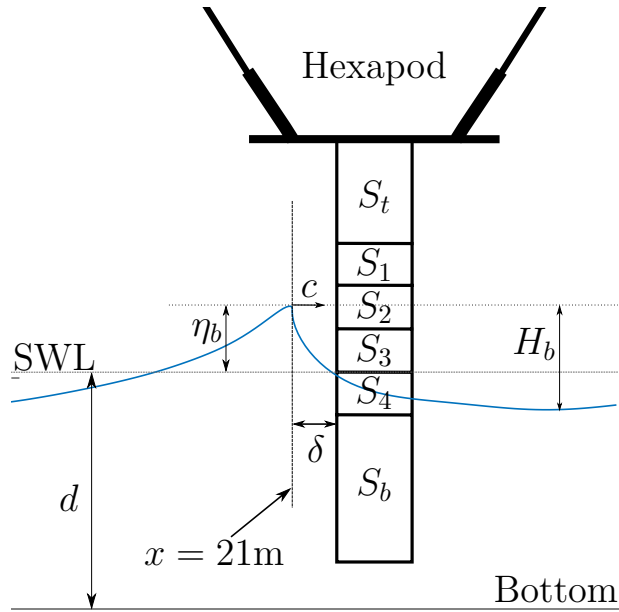


FIGURE 2 – Breaking wave impacting the mockup in the flume

kN nominal range on section S_4 . During the impact stage, the force signals are recorded at a frequency of 250 kHz with a GEN7 HBM recorder equipped with two input racks of type GN1640B. Each of these sections is made out of a central beam element and an outer part, called the skin. The central beam elements are screwed together and to the top section S_t and to the bottom section S_b . They form the backbone of the structure and are responsible for its stiffness. The skin parts consist in an aluminum cylinder 147 mm high, 40 cm in diameter and 1 cm thick. It is connected to the backbone via the force transducer. Consequently, the force transducers independently measure the force acting on each section. The gaps between the skin parts of the mockup are sealed with two layers of tape. One layer of surgical tape ensures the waterproofness and a second layer of white vinyl tape stiffens the assembly and allows marking. A marking composed of 5×5 cm² squares was drawn on the mockup (see figure 1) to qualitatively follow the interface between the water surface and the mockup.

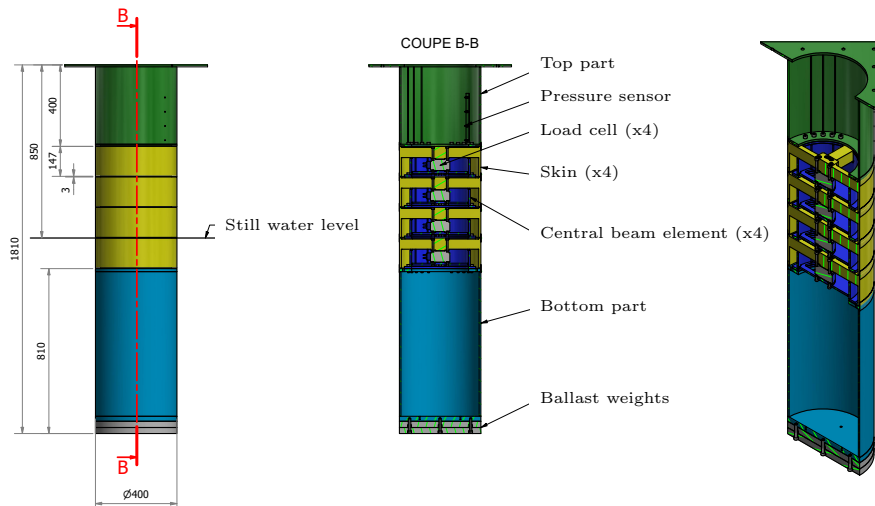


FIGURE 3 – Assembly drawing of the mockup

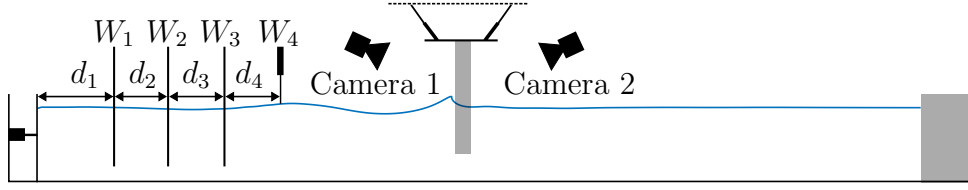


FIGURE 4 – General description of the experimental setup and instrumentation. The position of the wave gauges W_1 , W_2 , W_3 and W_4 are $d_1 = 10.099\text{m}$, $d_2 = 0.605\text{m}$, $d_3 = 0.598\text{m}$ and $d_4 = 0.593\text{m}$.

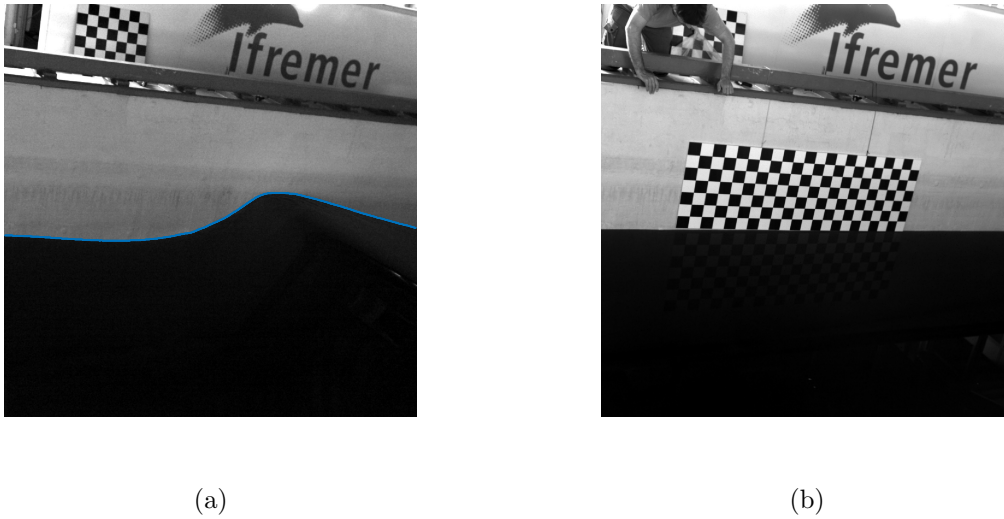


FIGURE 5 – (a) Detection of the free surface using the Canny filter. (b) Image of the checkerboard used to determine the flume coordinates of the water free surface.

II – 3 Additional sensors

Four wave gauges and two high-speed video cameras were used to follow the free surface evolution before and during the impact. These sensors are presented in figure 4. The wave gauges are located ten meters upstream of the mockup. They are used to check the agreement between the measured and modeled free surface elevations. During the impact, they were recorded with a sample frequency of 250 kHz. The two high-speed video cameras record the impact, one at the front and one at the rear of the mockup. They allow to track the interface between the mockup and the free surface.

II – 4 Experimental characterization of the breaking waves

An experimental characterization of the breaking waves was done without the cylinder using one high-speed video camera. The interface between the water free surface and the wall was filmed at 50 Hz and the corresponding points were identified using a Canny filter. An image obtained by the video camera is depicted in figure 5a. The identified free-surface points correspond to the blue crosses, which appear as a line due to the high number of points. The identified pixels were converted into the wave basin coordinates using a checkerboard installed on the wall of the basin. A picture of the checkerboard is depicted in figure 5b. The results obtained with this method are presented in section III – 2.

III – Breaking wave generation

The generation of waves breaking at a precise location was done iteratively using phase focusing. As it is complicated to precisely determine a breaking location experimentally, the breaking wave generation was carried out using the fully non-linear potential flow (FNPF) solver developed by S. Grilli [4]. The solver relies on the boundary element method (BEM) and fully non-linear boundary conditions.

III – 1 Breaking wave generation methodology

The breaking waves were generated through the focalisation of a Jonswap spectrum which higher frequencies were removed. The phase focusing method is presented by Rapp and Melville [9] and has been further reused by many authors. The waves are described using a first-order theory. The free surface elevation at a position x and a time t reads :

$$\eta(x, t) = \sum_{n=1}^N a_n \cos(k_n x - \omega_n t - \phi_n), \quad (1)$$

where ω_n and k_n satisfy the dispersion relation, a_n is the amplitude of the components which are defined by the considered spectrum and ϕ_n is the phase of the components. The phase focusing method consists in choosing ϕ_n so that at a given time t_{foc} and a given location x_{foc} , all the different components are at their maximum. Once the phases are determined, the free-surface elevation at $x = 0$ can be computed. The displacement of the piston wave generator is then obtained using the Biésel first order transfer function, description of which can be found in [1].

We define the position of breaking x_b as the position at which a part of the wave first becomes vertical. As first observed in [9], the actual position of breaking strongly depends on the values of the a_n components. Starting from small a_n values, no breaking is observed. If one gradually increases the wave amplitude, a small spilling breaker will first appear. In this case, breaking occurs downstream of the focusing location. If one continues to increase the wave amplitude, breaking will occur earlier and upstream of the focusing point. Eventually, a strong plunging breaker will be generated ahead of x_{foc} . One should note that even if the spectrum amplitude and the strength of breaking are related, it may happen that an increase in the wave amplitude leads to a gentler breaking earlier in time and space. The breaking location being different from the focusing point, obtaining breaking at the targeted location $x_{tar} = 21$ m requires to iteratively modify the focusing point as follows :

$$x_{foc}^{i+1} = x_{foc}^i - (x_b^i - x_{tar}), \quad (2)$$

where x_b^i is the breaking location obtained using the focus point x_{foc}^i . This procedure allows to shift the breaking location within a few centimeters of the desired breaking location x_{tar} . An accuracy of ± 0.1 m was deemed sufficient.

III – 2 Presentation of the generated breaking waves

Different truncated JONSWAP spectra low-pass filtered at 0.8 Hz were used to generate the breaking waves using the methodology presented in the previous section. Using a frequency discretization of 0.01 Hz, this led to consider 80 components. Low-pass filtering the spectra allows to eliminate early breakings generated by high frequencies. In the present paper we only present the results obtained for a particular breaker which corresponds to a mild plunging breaker and which was used to investigate the influence

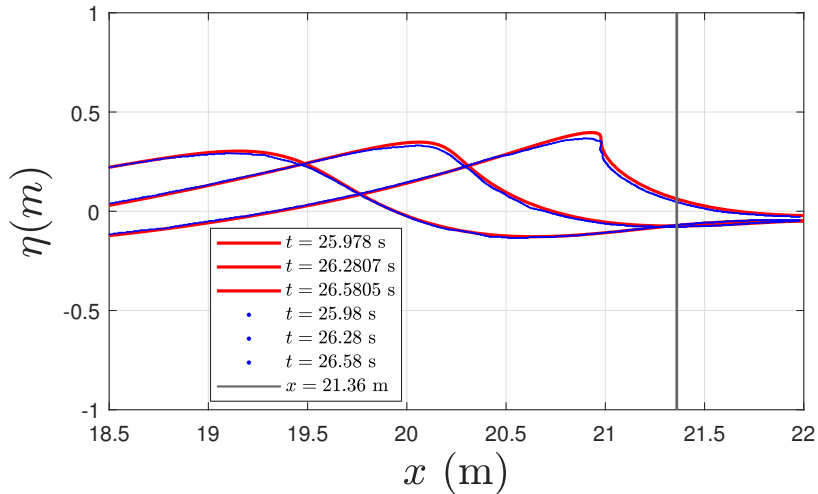


FIGURE 6 – Free surface profiles of the considered breaking wave at different instants computed using the FNPf solver (red lines) and the experimental procedure (blue dots). The vertical black line corresponds to a possible location of the front face of the cylinder.

	Experimental	FNPf
c_{crest} (m/s)	2,98	2.92
η_b (m)	0.37	0.40
x_b (m)	20.98	21.00
t_b (s)	26.56	26.59

TABLE 1 – Characteristics of the considered breaking wave : c_{crest} is the speed of the crest, η_b is the height of the breaking crest, x_b is the breaking location and t_b is the breaking time.

of several parameters. The breaker was obtained using a spectrum peak period T_p of 2.25 s and a peak enhancement factor γ of 3.3. The evolution of the breaker profile in time is depicted in figure 6. Both the free-surface profiles computed by the FNPf solver and the measured free-surface profiles are presented. The crest speed, c_{crest} , the crest elevation, η_b , the breaking location, x_b , and the breaking time, t_b , of the considered plunging breaker are given in table 1. The measured and modeled wave parameters are rather close. The main differences are observed at the crest : the measured crest elevation is smaller than the modeled crest elevation. Breaking occurs earlier in time and space according to the experimental data. This difference may be partly attributed to the measurement procedure. It was reported by Rapp and Melville [9] that breaking occurs earlier at the walls than in the middle of the flume.

IV – Analysis of the experimental data

In this section we present the results obtained during the breaking wave impact experiments in terms of hydrodynamic force. An example of the force signals recorded during an

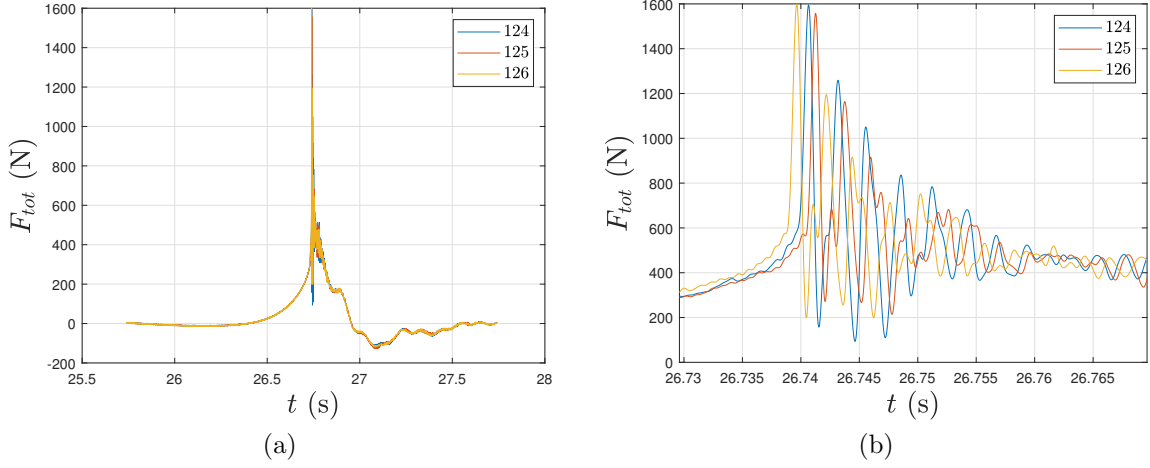


FIGURE 7 – (a) Sum of the forces measured in each of the sections. The force measured in each section was low-pass filtered using a high cutoff frequency $f_c = 1300$ Hz. (b) Zoom on the impact.

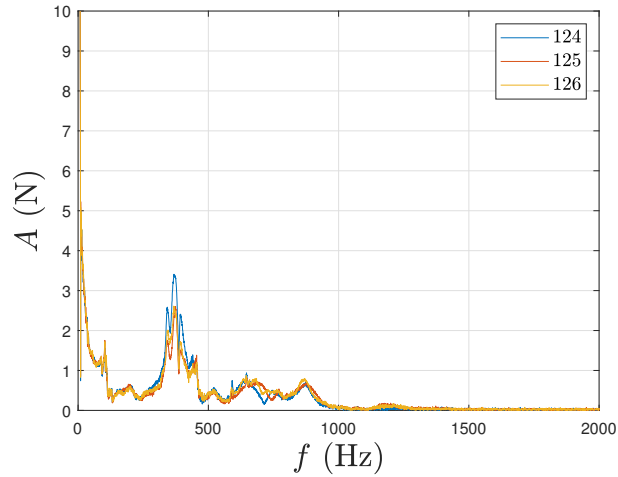


FIGURE 8 – Fourier transforms of the force signals presented in figure 7a

impact on the different sections is depicted in figure 7a. A zoomed-in view on the impact event is depicted in figure 7b. The different curves depicted in figures 7a and 7b correspond to the three repetitions of the same experimental conditions. Note that all experiments were repeated at least three times and that a calming down duration of 45 mn between each test was respected in order to ensure a good repeatability of the experiments. Nevertheless, a time shift of a few milliseconds is observed between the different runs, but a good repeatability is obtained in terms of maximum force. Strong oscillations on the impact force are present. The Fourier transforms of the three impact cases are depicted in figure 8. One can see that the force curves exhibit rather strong oscillations. They can be attributed to the vibrations of the skin parts due to the elasticity of the load cells and to the elasticity of the skin parts, as well as to the elastic vibrations of the backbone. A Fourier analysis of the different force signals is presented in figure 8, where one can observe different peaks corresponding to the different elastic modes of the skin parts. As a first approach, the force signals were low-pass filtered in order to reduce the effect of the vibrations. Figure 9 presents a comparison between the raw force measurements and the filtered data to which the components above 300 Hz were removed. This filtering allows

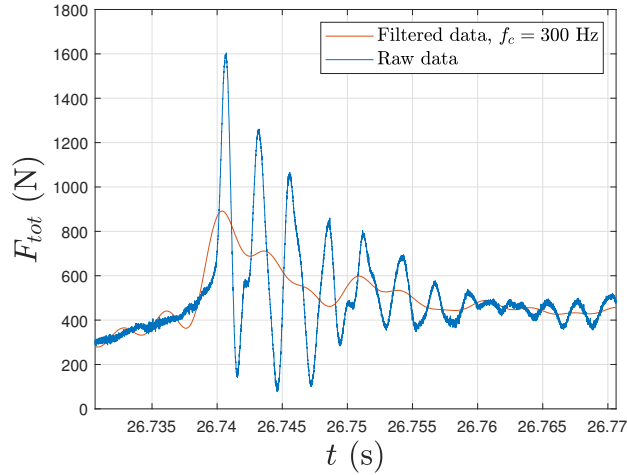


FIGURE 9 – Comparison of the raw measurements during a wave impact and the Fourier low-pass filtered measurements.

to remove an important part of the vibrations visible in the spectrum presented in figure 8, but it induces oscillations at the cutoff frequency which are clearly visible before and during the impact due to the so-called Gibbs phenomenon. Moreover, the high frequency part of the impact force is removed by the process. Throughout the article, data labelled *filtered* correspond to the data that was low-pass filtered at 300 Hz.

V – Influence of different parameters on impact loads

The influence of different parameters on the impact force was investigated. These parameters are the distance, δ , between the front face of the mockup and the breaking location, the pitch angle of the mockup, θ , and the horizontal velocity of the mockup, V .

V – 1 Effect of the distance between the mockup and the breaking location

Let δ be the distance between the front face of the mockup and $x = 21$ m, the target breaking location. This parameter is represented in figure 2. It is of practical importance for two reasons. First, as it will be shown below, the value of the maximum impact force strongly depends on δ . Secondly, it determines an interval for the structure location within which impact may occur. During the experimental campaign, the influence of δ was varied from 0.06 m to 0.66 m. The evolution of the impact force with δ is depicted in figure 10. One can see that a sharp rise of the measured impact force appears for $\delta = 0.18$ m. This rise is explained by the increase of the impact force, as well as by the increase of the structural response. One can see that the dispersion in the measurements is much higher in the transition between the low impact force regime and the high impact force regime. A plateau is observed between 0.25 and 0.5 m. After 0.5 m, a slow decay of the impact force is observed.

V – 2 Influence of the horizontal speed of the mockup

The influence of the horizontal speed of the mockup at impact was investigated. The kinematics of the mockup was defined so that impact occurs at the same instant and location for all speeds. At this time, the mockup velocity is constant. The setpoints for

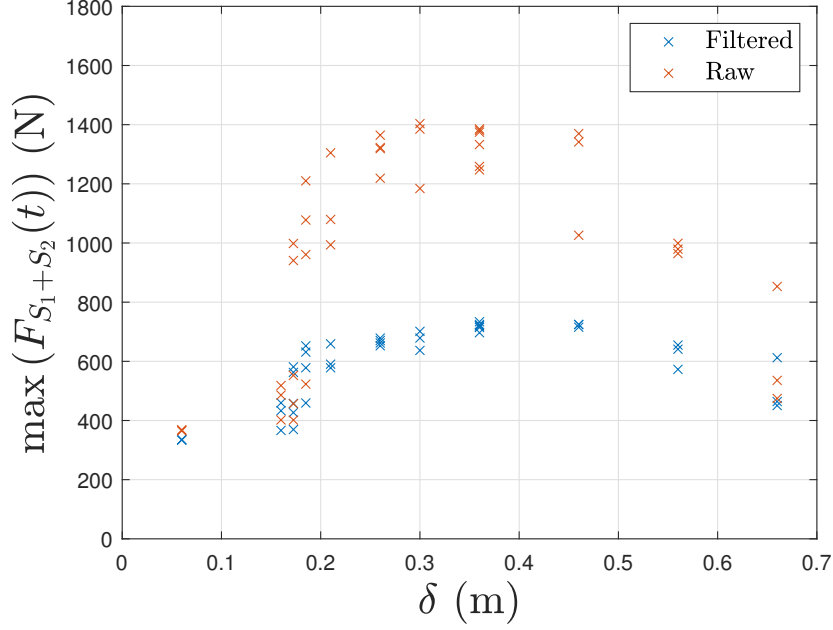


FIGURE 10 – Maximum force measured on the 2 sections during wave impacts at different positions. The maximum was computed on the raw force measurements as well as on the low-pass filtered force measurements.

the mockup position are shown in figure 11. The mockup position is a sine to which a constant velocity part was added. The sine period was taken equal to two seconds. The sine amplitude is taken so that when the sine second derivative is equal to zero, its first derivative is equal to the desired mockup velocity. A phase of constant velocity is added at this instant. This phase is highlighted in orange in figure 11. The time of impact t_i was identified during an impact with zero velocity at the position x_i and corresponds to the time instant at which the impact force is maximum. The motions of the mockup and the wave generator were synchronized so that the mockup is at position x_i at instant t_i for the different velocity cases. The target impact time is depicted in figure 11 by the black vertical line. Two different mockup velocities were investigated : 0.4 and 0.8 m/s. Note that the movement of the mockup is in the same direction as the wave propagation. The evolution of the maximum impact force as a function of the mockup velocity is depicted in figure 12a. Figure 12b shows the maximum impact force divided by $0.5\eta_b\rho R(c_{crest} - V)^2$, c_{crest} being the crest velocity predicted by the FNPF solver. This corresponds to the non-dimensional impact force coefficient based on the relative speed between the wave crest and the mockup. Figure 12b shows that the resulting slamming coefficient is almost a constant, which supports the assumption that an impact on a moving cylinder is equivalent to an impact at the relative speed. An arbitrary height of impact equal to $0.5\eta_b$ was fixed to obtain the non-dimensional slamming coefficient. Even though more points would be required for a robust conclusion, it appears that the slamming coefficient is not very sensitive to the impact velocity.

V – 3 Influence of the pitch angle of the mockup

The influence of the pitch angle of the mockup, θ , was investigated. The centre of rotation of the mockup is the intersection between the still water level and the axis of the cylinder, as shown in figure 13. A positive value of θ corresponds to an inclination of the mockup in the direction of wave propagation. The evolution of the maximum force

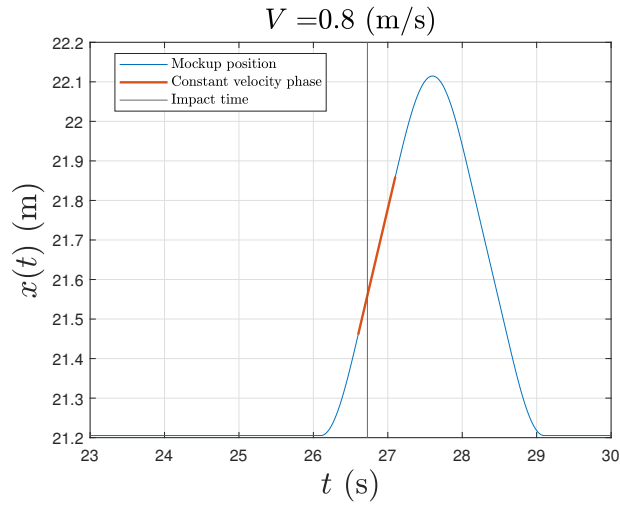


FIGURE 11 – Time evolution of the horizontal mockup position.

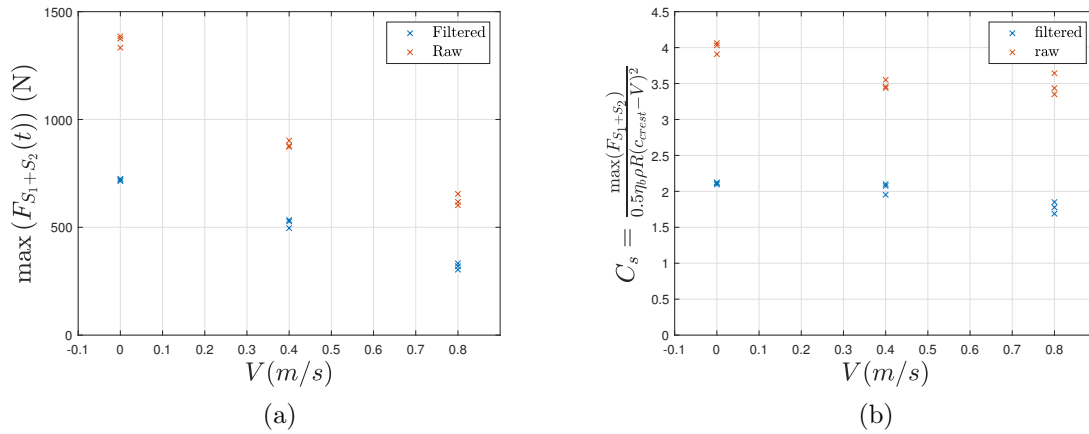


FIGURE 12 – (a) Evolution of the maximum measured force on the two upper sections with the horizontal mockup velocity. (b) Evolution of the slamming coefficient with the horizontal mockup velocity.

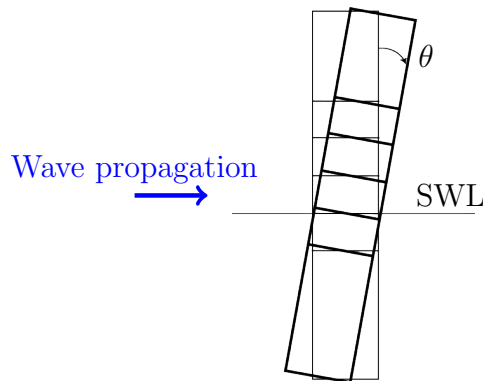


FIGURE 13 – Pitch angle of the mockup. The centre of rotation corresponds to the intersection between the still water level and the axis of the mockup.

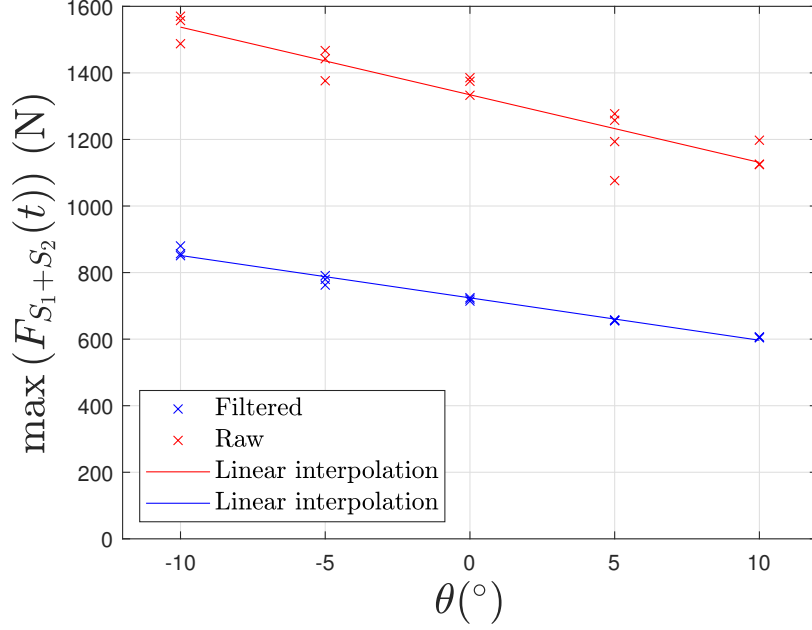


FIGURE 14 – Maximum force measured on the 2 upper sections during wave impacts with different pitch angles. The maximum was computed on the raw force measurements as well as on the 300 Hz low-pass filtered force measurements.

measured on the two upper sections is depicted in figure 14. A linear approximation was fitted to the raw and filtered data. It appears that in the considered range of inclinations, it seems reasonable to consider that the force evolves linearly with the pitch angle. The rotation being made around the intersection between the cylinder axis and the still water level, one should note that such a rotation induces a displacement of the upper sections with respect to the breaking location. For instance, a rotation of 10° induces a 5 cm displacement 30 cm above the free surface. Therefore, comparisons with the results obtained by Wienke and Oumeraci [14] are difficult due to the different choice for the point of rotation. In [14], the rotation is made around a point situated at the bottom of the flume, which is 4 m deep. In this case, a rotation of 10° induces a shift of 0.9 m at 1 m above the free surface. The displacement of the impact location with respect to the breaking location may thus be as important as the influence of the pitch angle in the experiments of [14]. In our case, the impact case with no pitch angle of the mockup corresponds to a distance $\delta = 0.36$ m. This location is situated on the plateau of figure 10. The 5 cm shift of the breaking location should thus be of minor importance in the evolution of the maximum impact force.

VI – Conclusions

During the first DIMPACT experimental campaign, wave impacts were carried out on a segmented cylinder mounted on an hexapod. The effects of the mockup attitude and velocity on the impact force were studied. Three parameters were investigated : the distance δ between the breaking location and the front face of the cylinder, the pitch angle of the mockup and its horizontal velocity. The distance δ appears to be the main parameter affecting impact loads. For the considered wave, a strong increase of the impact force is observed for $\delta \geq 0.18$ m. A plateau is observed for higher values followed by a slow decrease of the maximum impact force. During an upcoming second experimental campaign, efforts

will be set on determining this evolution for other impact cases, in particular spilling breakers. Impacts on a moving mockup show that the maximum impact force depends on the square of the relative velocity between the wave crest and the mockup. More data would be needed to draw further conclusions. Experiments with an inclined cylinder highlight a linear dependence between the maximum impact force and the pitch angle of the mockup.

Acknowledgements

This work benefited from government support managed by the Agence Nationale de la Recherche under the program Investissements d’Avenir with the reference ANR-10-IEED-06-34 related to the DIMPACT project. The authors are grateful to S. Grilli for providing the FNPF solver and providing useful insights on its use. We would also like to thank C. Peyrard and M. Telles from EDF for determining the mockup attitudes that were investigated during the experimental campaign.

Références

- [1] T. L. Andersen and P. Frigaard. *Wave Generation in Physical Models : Technical documentation for AwaSys 6*. Number 34 in DCE Lecture notes. Department of Civil Engineering, Aalborg University, Denmark, 2014.
- [2] A. Antonini, J. M. William Brownjohn, D. Dassanayake, A. Raby, J. Bassit, A. Pappas, and D. D’Ayala. A Bayesian inverse dynamic approach for impulsive wave loading reconstruction : Theory, laboratory and field application. *Coastal Engineering*, 168 :103920, Sept. 2021.
- [3] J. M. Esandi, E. Buldakov, R. Simons, and D. Stagonas. An experimental study on wave forces on a vertical cylinder due to spilling breaking and near-breaking wave groups. *Coastal Engineering*, 162 :103778, 2020. Publisher : Elsevier.
- [4] S. T. Grilli and R. Subramanya. Numerical modeling of wave breaking induced by fixed or moving boundaries. *Computational Mechanics*, 17(6) :374–391, Apr. 1996.
- [5] H. F. Hansen and H. Kofoed-Hansen. An engineering-model for extreme wave-induced loads on monopile foundations. In *ASME 2017 36th International Conference on Ocean, Offshore and Arctic Engineering*. American Society of Mechanical Engineers Digital Collection, 2017.
- [6] G. Lian. *Slamming loads on large volume structures from breaking waves*. PhD Thesis, University of Stavanger, 2018.
- [7] R. Manjula, S. A. Sannasiraj, and K. Palanichamy. Laboratory Measurements of Breaking Wave Impact Pressures on a Slender Cylindrical Member. *The International Journal of Ocean and Climate Systems*, 4(3) :151–169, 2013. eprint : <https://doi.org/10.1260/1759-3131.4.3.151>.
- [8] B. T. Paulsen, B. d. Sonnevile, M. v. d. Meulen, and N. G. Jacobsen. Probability of wave slamming and the magnitude of slamming loads on offshore wind turbine foundations. *Coastal Engineering*, 143 :76–95, 2019.
- [9] R. J. Rapp and W. K. Melville. Laboratory measurements of deep-water breaking waves. *Philosophical Transactions of the Royal Society of London. Series A, Mathematical and Physical Sciences*, 331(1622) :735–800, 1990. Publisher : The Royal Society London.

- [10] S. Saincher, V. Sriram, S. Agarwal, and T. Schlurmann. Experimental investigation of hydrodynamic loading induced by regular, steep non-breaking and breaking focused waves on a fixed and moving cylinder. *European Journal of Mechanics - B/Fluids*, 93 :42–64, May 2022.
- [11] T. Sawaragi and M. Nochino. Impact Forces of Nearly Breaking Waves on a Vertical Circular Cylinder. *Coastal Engineering in Japan*, 27(1) :249–263, Dec. 1984. Publisher : Taylor & Francis.
- [12] L. Suja-Thauvin, J. R. Krokstad, E. E. Bachynski, and E.-J. de Ridder. Experimental results of a multimode monopile offshore wind turbine support structure subjected to steep and breaking irregular waves. *Ocean Engineering*, 146 :339–351, 2017. Publisher : Elsevier.
- [13] M. H. Vested, S. Carstensen, and E. D. Christensen. Experimental study of wave kinematics and wave load distribution on a vertical circular cylinder. *Coastal Engineering*, 157 :103660, Apr. 2020.
- [14] J. Wienke and H. Oumeraci. Breaking wave impact force on a vertical and inclined slender pile—theoretical and large-scale model investigations. *Coastal Engineering*, 52(5) :435–462, May 2005.
- [15] D. Zhou, E. S. Chan, and W. K. Melville. Wave impact pressures on vertical cylinders. *Applied Ocean Research*, 13(5) :220–234, Oct. 1991.